Journal of Sound and Vibration (1997) **202**(4), 477–490

NON-LINEAR ACTIVE VIBRATION CONTROL OF A CANTILEVER PIPE CONVEYING FLUID

Y.-H. Lin and Y.-K. Tsai

Department of Mechanical and Marine Engineering, National Taiwan Ocean University, Keelung, Taiwan 20224, *Republic of China*

(*Received* 2 *July* 1996, *and in final form* 6 *November* 1996)

Active vibration suppression of a fluid conveying cantilever pipe with geometric non-linearity due to post-critical flow speed is examined. The non-linear characteristics of the system is described using the fictitious load approach and the dynamic responses can be obtained using successive co-ordinate transformations, which only require the solution of linear differential equations, without the need to deal with the complex non-linear strain–displacement relationships. An instantaneous optimal closed loop control approach by minimizing an objective function at each time instant is developed using the Newmark method for solution of the linear equations of motion. The effect of actuator location on the performance of the control system is described. It is demonstrated that the control design is also applicable for vibration suppression of the fluid conveying cantilever pipe subjected to random base excitations.

1. INTRODUCTION

The literature concerning the dynamics of fluid conveying pipes is abundant. Since the early work by Housner [1], there have been over two hundred articles dealing with the subject [2]. The analysis has been shown to be important in the design of structural systems subjected to high fluid flow disturbance, such as nuclear reactor components [3], the feed line of rocket motors [4] and piping systems [5]. It is observed from linear analysis [1, 6, 7] that for a pipe with supported ends, the system loses stability by divergence, whereas for cantilever pipes, the instability is of the flutter type. However, linear models are found to be in serious error when the flow speed exceeds the critical value, and the structure undergoes large deformations, which are non-linear in nature for analysis [8]. The dynamic behavior of pipes conveying fluid near the critical velocity has been analyzed considering the effects of large deformations [9]. For post-critical flow speeds, some of the non-linear terms discarded in [9] need to be re-examined. A Galerkin finite element approach was applied for fluid conveying pipes with post-critical flow speeds [10]. A penalty parameter, which is problem dependent, must be correctly chosen to ensure numerical stability.

Intense research efforts have been made to assess the dynamic characteristics of pipes conveying fluid. However, the literature on vibration control of fluid conveying pipes is quite limited. The study is important to prevent system failure due to fatigue and to ensure operational accuracy. Tani and Sudani [11, 12] reported a sub-optimal control law for vibration suppression of fluid conveying tubes by using motor controlled tendons. Kangaspuoskari *et al*. [13] examined the effect of feedback control on critical velocity of cantilevered pipes aspirating fluid. A robust flutter control approach for a vertical pipe

0022–460X/97/190477 + 14 $25.00/0/sv960858

conveying fluid using a gyroscopic mechanism was reported by Cui *et al*. [14]. Lin and Chu [15] applied the optimal independent modal space control approach for active vibration suppression of a cantilever pipe conveying fluid by using piezoelectric actuators. In all of these analyses, it was assumed that the plant is linear; that is, vibration of the pipe is small. This work is concerned with the numerical evaluations of an instantaneous optimal control design for vibration control of pipes conveying fluid with a post-critical flow speed. A large vibration amplitude, which results in geometric non-linearity, is considered. Optimal control of non-linear civil structures was reported by minimizing an objective function at every time instant [16]. The non-linear damping and elastic forces were truncated by using the first order approximation, and tangent damping and stiffness matrices were formulated accordingly. A procedure for static large deformation analysis of slender frame structures using the concept of fictitious loads was developed [17]. Only linear equations need to be solved. The static large deformation of the structures can be computed by iteratively updating the finite element nodal co-ordinates, without the need to formulate the non-linear strain–displacement relationship. In this work, the concept of fictitious loads is extended to describe the dynamic behavior of cantilever pipes conveying fluid with post-critical flow velocities. Instantaneous optimal closed loop control for vibration suppression of a cantilever pipe conveying fluid is developed, taking into account the non-linear dynamic characteristics of the system. The formulation of tangent damping and stiffness matrices is no longer necessary in this development. The linear equations of motion are solved using the Newmark method [18], which simplifies the control system design.

2. MODEL FORMULATION

The equation of motion for a cantilever pipe conveying fluid exhibiting large deformations at any instant t can be expressed as

$$\mathbf{M}^t\ddot{\mathbf{D}}^t + \mathbf{C}^t\dot{\mathbf{D}}^t + \mathbf{K}^t\mathbf{D}^t = \mathbf{R}^t, \tag{1}$$

where $\mathbf{M}^t$ is the structural mass matrix, $\mathbf{C}^t$ is the structural damping matrix, $\mathbf{K}^t$ is the structural stiffness matrix, $\mathbf{R}^t$ is the structural forcing vector, and $\mathbf{D}^t$, $\dot{\mathbf{D}}^t$ and $\ddot{\mathbf{D}}^t$ denote the structural displacement, velocity and acceleration vectors respectively. In this work the approach by using fictitious forces as developed by Kohnke [17] for static analyses is extended for describing the dynamic behavior of the fluid conveying cantilever pipe. The procedure is based on the Eulerian approach, which does not require the evaluation of non-linear strain–displacement relationships. Kinematic corrections due to the large deformation of the pipe are accounted for using fictitious loads. The nodal co-ordinates are updated during the course of computation by using co-ordinate transformation. The complex procedure for formation of the non-linear structural matrix equations is no longer required. The structural matrices shown above can be written as

$$\mathbf{M}^t = \sum_{j=1}^{n} \mathbf{T}^{\mathrm{T}}\mathbf{m}_{l_e}\mathbf{T}_j, \qquad \mathbf{C}^t = \sum_{j=1}^{n} \mathbf{T}_j^{\mathrm{T}}\mathbf{c}_{l_e}\mathbf{T}_j,$$

$$\mathbf{K}^t = \sum_{j=1}^{n} \mathbf{T}_j^{\mathrm{T}}\mathbf{k}_{l_e}\mathbf{T}_j, \qquad \mathbf{R}^t = \sum_{j=1}^{n} \mathbf{T}_j^{\mathrm{T}} r_{l_j}, \tag{2a}$$

in which n is the number of elements used, the superscript $\mathbf{T}$ denotes the transpose of a

matrix, $\mathbf{r}_{l_j}$ is the element load vector, and the co-ordinate transformation matrix is given as

$$\mathbf{T}_j = \begin{bmatrix} \cos\theta_j & \sin\theta_j & 0 & 0 & 0 & 0 \\ -\sin\theta_j & \cos\theta_j & 0 & 0 & 0 & 0 \\ 0 & 0 & 1 & 0 & 0 & 0 \\ 0 & 0 & 0 & \cos\theta_j & \sin\theta_j & 0 \\ 0 & 0 & 0 & -\sin\theta_j & \cos\theta_j & 0 \\ 0 & 0 & 0 & 0 & 0 & 1 \end{bmatrix}. \tag{2b}$$

Also,

$$\mathbf{m}_{l_e} = \mathbf{m}_{p_e} + \mathbf{m}_{f_e}, \qquad \mathbf{c}_{l_e} = \mathbf{c}_{f_e}, \qquad \mathbf{k}_{l_e} = \mathbf{k}_{p_e} + \mathbf{k}_{f_e}. \tag{2c}$$

where $\mathbf{m}_{p_e}$ and $\mathbf{k}_{p_e}$ denote the element mass and stiffness matrices of the pipe, respectively; and $\mathbf{m}_{f_e}$, $\mathbf{c}_{f_e}$, and $\mathbf{k}_{f_e}$ represent the fluid element mass, damping and stiffness matrices, respectively. Internal damping of the pipe is considered to be small and is neglected. For completeness, the formulation of the element matrices for both the pipe and fluid is given in the Appendix. The Newmark method [18] is used to develop the procedure for instantaneous optimal control of the cantilever pipe conveying fluid exhibiting large deformations. The effective structural stiffness matrix and the effective structural load vector can be written, respectively, as

$$\hat{\mathbf{K}}^t = \mathbf{K}^t + a_0\mathbf{M}^t + a_1\mathbf{C}^t, \tag{3}$$

$$\hat{\mathbf{R}}^{t+\Delta t} = \mathbf{R}^{t+\Delta t} + \mathbf{M}^t(a_0\mathbf{D}^t + a_2\dot{\mathbf{D}}^t + a_3\ddot{\mathbf{D}}^t) + \mathbf{C}^t(a_1\mathbf{D}^t + a_4\dot{\mathbf{D}}^t + a_5\ddot{\mathbf{D}}^t), \tag{4}$$

where the integration constants are

$$a_0 = \frac{1}{\alpha\Delta t^2}, \qquad a_1 = \frac{\delta}{\alpha\Delta t}, \qquad a_2 = \frac{1}{\alpha\Delta t}, \qquad a_3 = \frac{1}{2\alpha} - 1,$$

$$a_4 = \frac{\delta}{\alpha} - 1, \qquad a_5 = \frac{\Delta t}{2}\left(\frac{\delta}{\alpha} - 2\right), \tag{5}$$

in which Δt is the integration time step; δ and α are chosen to be 0·5 and 0·25 respectively for numerical stability considerations. The structural displacement, acceleration, and velocity vectors at the instant $t + \Delta t$ can be computed as follows:

$$\mathbf{D}^{t+\Delta t} = (\hat{\mathbf{K}}^t)^{-1}\hat{\mathbf{R}}^{t+\Delta t}, \tag{6}$$

$$\ddot{\mathbf{D}}^{t+\Delta t} = a_0(\mathbf{D}^{t+\Delta t} - \mathbf{D}^t) - a_2\dot{\mathbf{D}}^t - a_3\ddot{\mathbf{D}}^t, \tag{7}$$

$$\dot{\mathbf{D}}^{t+\Delta t} = \dot{\mathbf{D}}^t + a_6\ddot{\mathbf{D}}^t + a_7\ddot{\mathbf{D}}^{t+\Delta t}, \tag{8}$$

where

$$a_6 = \Delta t(1 - \delta), \qquad a_7 = \delta\Delta t. \tag{9}$$

To facilitate the control formulation, equations (3)–(9) are combined to form the following equations expressed in state space:

$$\begin{Bmatrix} \mathbf{D}^{t+\Delta t} \\ \dot{\mathbf{D}}^{t+\Delta t} \end{Bmatrix} = \begin{bmatrix} \mathbf{A}_1 & \mathbf{A}_2 \\ \mathbf{A}_5 & \mathbf{A}_6 \end{bmatrix} \begin{Bmatrix} \mathbf{D}^t \\ \dot{\mathbf{D}}^t \end{Bmatrix} + \begin{Bmatrix} \mathbf{A}_3 \\ \mathbf{A}_7 \end{Bmatrix} \mathbf{R}^t + \begin{Bmatrix} \mathbf{A}_4 \\ \mathbf{A}_8 \end{Bmatrix} \mathbf{R}^{t+\Delta t}, \tag{10}$$

where

$$\mathbf{A}_1 = (\hat{\mathbf{K}}^t)^{-1}[a_0\mathbf{M}^t - a_3\mathbf{K}^t + a_1\mathbf{C}^t - a_5\mathbf{C}^t(\mathbf{M}^t)^{-1}\mathbf{K}^t],$$

$$\mathbf{A}_2 = (\hat{\mathbf{K}}^t)^{-1}[a_2\mathbf{M}^t - a_3\mathbf{C}^t + a_4\mathbf{C}^t - a_5\mathbf{C}^t(\mathbf{M}^t)^{-1}\mathbf{C}^t],$$

$$\mathbf{A}_3 = (\hat{\mathbf{K}}^t)^{-1}[a_3\mathbf{I} + a_5\mathbf{C}^t(\mathbf{M}^t)^{-1}], \qquad \mathbf{A}_4 = (\hat{\mathbf{K}}^t)^{-1},$$

$$\mathbf{A}_5 = (a_7a_3 - a_6)(\mathbf{M}^t)^{-1}\mathbf{K}^t + a_7a_0\mathbf{A}_1 - a_7a_0\mathbf{I},$$

$$\mathbf{A}_6 = \mathbf{I} + (a_7a_3 - a_6)(\mathbf{M}^t)^{-1}\mathbf{C}^t + a_7a_0\mathbf{A}_2 - a_7a_2\mathbf{I},$$

$$\mathbf{A}_7 = (a_6 - a_7a_3)(\mathbf{M}^t)^{-1} + a_7a_0\mathbf{A}_3, \qquad \mathbf{A}_8 = a_7a_0\mathbf{A_4}. \tag{11}$$

The structural load vector contains both the external forces, which includes the fictitious loads, and the active control input

$$\mathbf{R}^t = \mathbf{H}\mathbf{F}^t + \mathbf{R}_f^t, \qquad \mathbf{R}^{t+\Delta t} = \mathbf{H}\mathbf{F}^{t+\Delta t} + \mathbf{R}_f^{t+\Delta t}, \tag{12}$$

where $\mathbf{H}$ ($n \times r$) is the control output matrix, $\mathbf{F}$ ($r \times 1$) is the control force vector, and $\mathbf{R}_f$ ($n \times 1$) is the external force vector. The following equation is used to simplify the notations:

$$\mathbf{Y}^{t+\Delta t} = \mathbf{N}_1^t\mathbf{Y}^t + \mathbf{N}_2^t(\mathbf{H}\mathbf{F}^t + \mathbf{R}_f^t) + \mathbf{N}_3^t(\mathbf{H}\mathbf{F}^{t+\Delta t} + \mathbf{R}_f^{t+\Delta t}), \tag{13}$$

where

$$\mathbf{Y}^{t+\Delta t} = \begin{Bmatrix}\mathbf{D}^{t+\Delta t}\\ \dot{\mathbf{D}}^{t+\Delta t}\end{Bmatrix}, \qquad \mathbf{Y}^t = \begin{Bmatrix}\mathbf{D}^t\\ \dot{\mathbf{D}}^t\end{Bmatrix},$$

$$\mathbf{N}_1^t = \begin{bmatrix}\mathbf{A}_1 & \mathbf{A}_2\\ \mathbf{A}_5 & \mathbf{A}_6\end{bmatrix}, \qquad \mathbf{N}_2^t = \begin{Bmatrix}\mathbf{A}_3\\ \mathbf{A}_7\end{Bmatrix},$$

$$\mathbf{N}_3^t = \begin{Bmatrix}\mathbf{A}_4\\ \mathbf{A}_8\end{Bmatrix}. \tag{14}$$

3. INSTANTANEOUS OPTIMAL CLOSED LOOP CONTROL

The objective function to be minimized to formulate the instantaneous optimal control algorithms is defined as

$$J^{t+\Delta t} = \mathbf{Y}^{t+\Delta t^{\mathrm{T}}}\mathbf{Q}\mathbf{Y}^{t+\Delta t} + \mathbf{F}^{t+\Delta t^{\mathrm{T}}}\mathbf{W}\mathbf{F}^{t+\Delta t}, \tag{15}$$

where $\mathbf{Q}$ and $\mathbf{W}$ are the weighting matrices for the state vector and the active control force vector, respectively. The Hamiltonian is obtained by introducing a Lagrangian multiplier vector $\mathbf{p}^{t+\Delta t}$ to the objective function:

$$H^{t+\Delta t} = \mathbf{Y}^{t+\Delta t^{\mathrm{T}}}\mathbf{Q}\mathbf{Y}^{t+\Delta t} + \mathbf{F}^{t+\Delta t^{\mathrm{T}}}\mathbf{W}\mathbf{F}^{t+\Delta t} + \mathbf{p}^{t+\Delta t^{\mathrm{T}}}[\mathbf{Y}^{t+\Delta t} - \mathbf{N}_1^t\mathbf{Y}^t - \mathbf{N}_2^t(\mathbf{H}\mathbf{F}^t + \mathbf{R}_f^t) - \mathbf{N}_3^t(\mathbf{H}\mathbf{F}^{t+\Delta t} + \mathbf{R}_f^{t+\Delta t})]. \tag{16}$$

The necessary conditions for minimizing the objective function given in equation (15) subject to the constraint equation (13) can be written as [19]

$$\frac{\partial H^{t+\Delta t}}{\partial \mathbf{Y}^{t+\Delta t}} = 0, \qquad \frac{\partial H^{t+\Delta t}}{\partial \mathbf{F}^{t+\Delta t}} = 0, \qquad \frac{\partial H^{t+\Delta t}}{\partial \mathbf{p}^{t+\Delta t}} = 0. \tag{17}$$

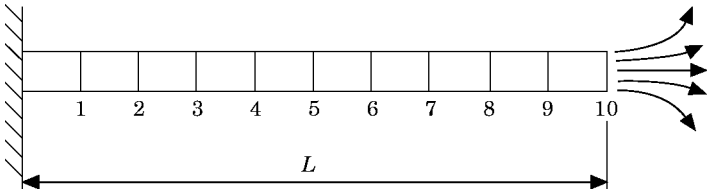

Figure 1. The finite element model of a cantilever pipe conveying fluid, with the fluid discharging at the right end.

The following two equations can be obtained by substituting equation (16) into the first two expressions in equation (17):

$$\mathbf{2QY}^{t+\Delta t} + \mathbf{p}^{t+\Delta t} = 0, \tag{18}$$

$$2\mathbf{WF}^{t+\Delta t} - \mathbf{HN}_3^{t\mathrm{T}}\mathbf{p}^{t+\Delta t} = 0. \tag{19}$$

Note that the third expression in equation (17) yields an identical expression as in equation (13). The Lagangian multiplier vector is regulated by the feedback state vector for a closed loop control; that is,

$$\mathbf{p}^{t+\Delta t} = \eta \mathbf{Y}^{t+\Delta t}. \tag{20}$$

Substituting equation (20) into equation (18) and knowing that the state vector cannot be identically zero, the unknown matrix η can be obtained. The control force vector can then be obtained as below by using equation (19):

$$\mathbf{F}^{t+\Delta t} = -\mathbf{W}^{-1}\mathbf{H}^{\mathrm{T}}\mathbf{N}_3^{t\mathrm{T}}\mathbf{QY}^{t+\Delta t}. \tag{21}$$

4. NUMERICAL RESULTS

In Figure 1 is shown a cantilever pipe conveying fluid with ten elements, used to describe the model. The numerical data, as used in reference [10], for analysis are as follows:

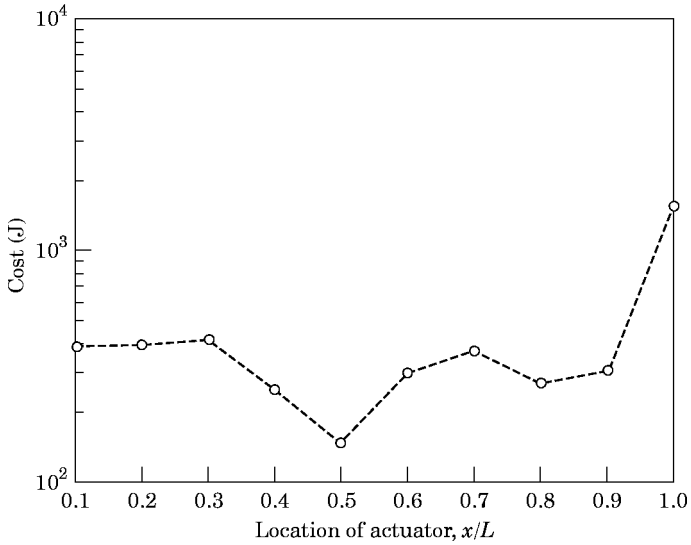

Figure 2. The effect of actuator location on the vibration control cost of the cantilever pipe conveying fluid; flow speed 22 m/s, integration time step 0·001 s, simulation time length 0·9 s and weighting parameter $Q^*/W = 1$.

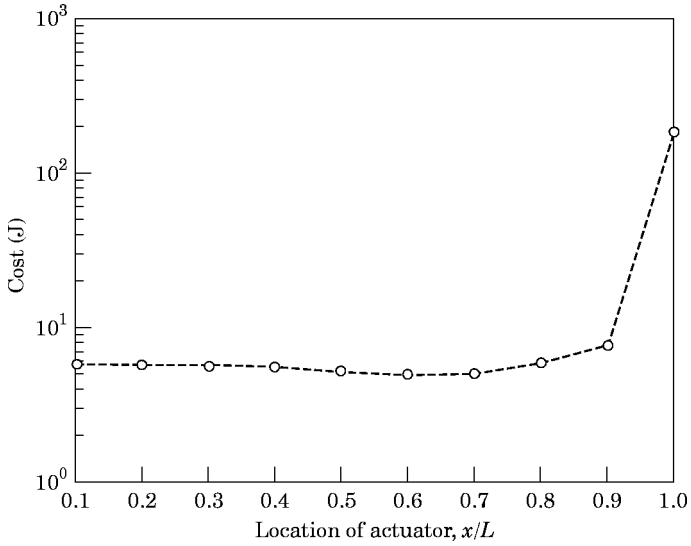

Figure 3. The effect of actuator location on the vibration control cost of the cantilever pipe conveying fluid; flow speed 18 m/s, other values as in Figure 2.

Young's modulus 2·5217e8 Pa, pipe length 0·6858 m, outside diameter 9·525e − 3 m, pipe thickness 1·5875e − 3 m, mass density 852·59 kg/m^3, and fluid mass density 1000 kg/m^3. An active control moment is considered as the control input, which can be realized either by using the piezoelectric ceramics as described in [15] or by using the motor controlled tendon mechanism, as presented in [11]. The cost, as defined in equation (15), for various positions of the active control input are illustrated in Figures 2 and 3 with flow speeds of 22 m/s

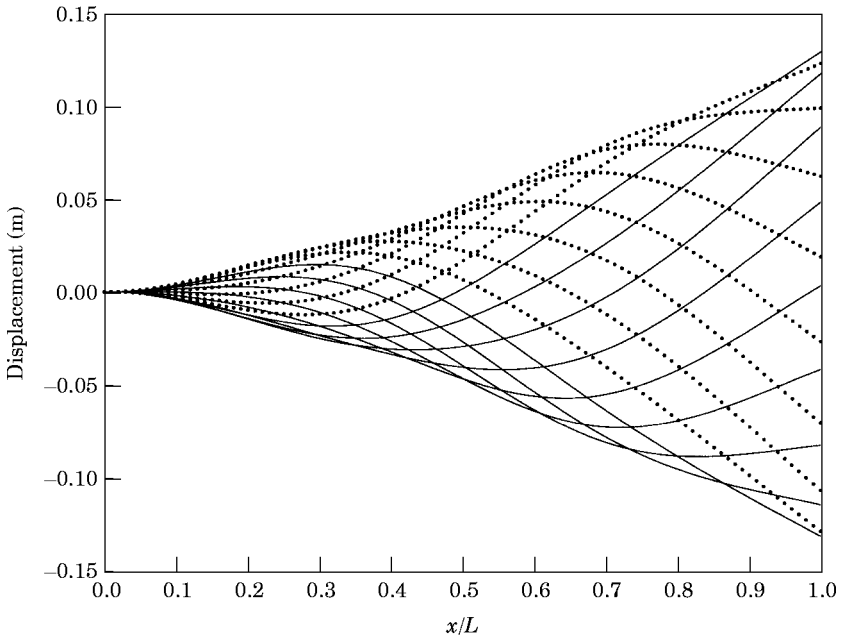

Figure 4. One vibration cycle of the transverse displacement of the cantilever pipe conveying fluid with a flow speed of 22 m/s. ——, Downward motion; ···, upward motion.

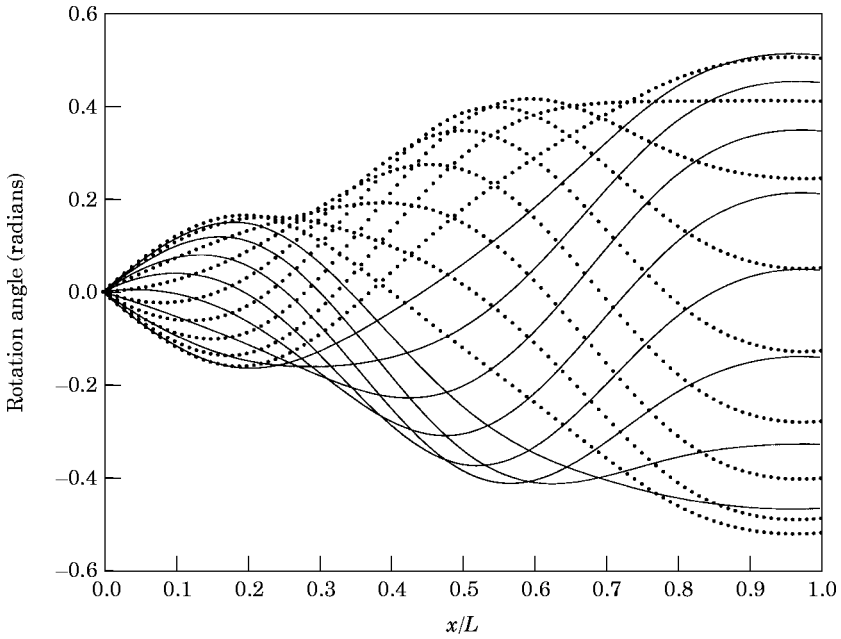

Figure 5. One vibration cycle of the rotational displacement of the cantilever pipe conveying fluid with a flow speed of 22 m/s. ——, Downward motion; ···, upward motion.

and 18 m/s respectively. The critical flow speed can be shown to be 21·2 m/s. The integration step is 0·001 s and simulation time length is 0·9 s. The weighting matrix parameter selected is $Q^*/W = 1$, where $\mathbf{Q}_d = Q^*\mathbf{I}$, $\mathbf{Q} = \text{diag}\,(\mathbf{Q}_d\ \mathbf{0})$, and $\mathbf{I}$ is an identity

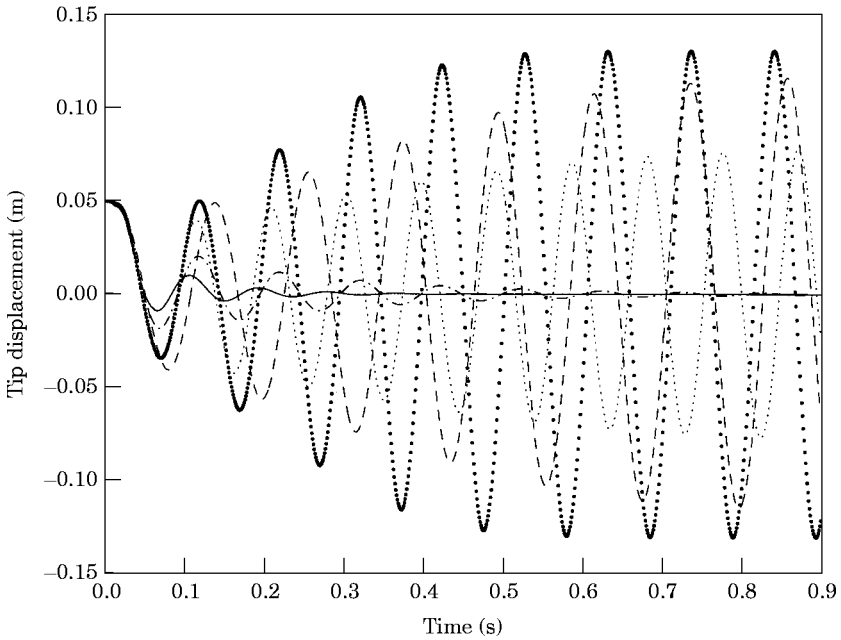

Figure 6. The vertical tip responses for various actuator locations with a flow speed of 22 m/s and a weighting parameter of $Q^*/W = 6$. ●●●, Uncontrolled; – – –, $x/L = 0{\cdot}7$; ···, $x/L = 0{\cdot}2$; –·–, $x/L = 0{\cdot}4$; ——, $x/L = 0{\cdot}5$.

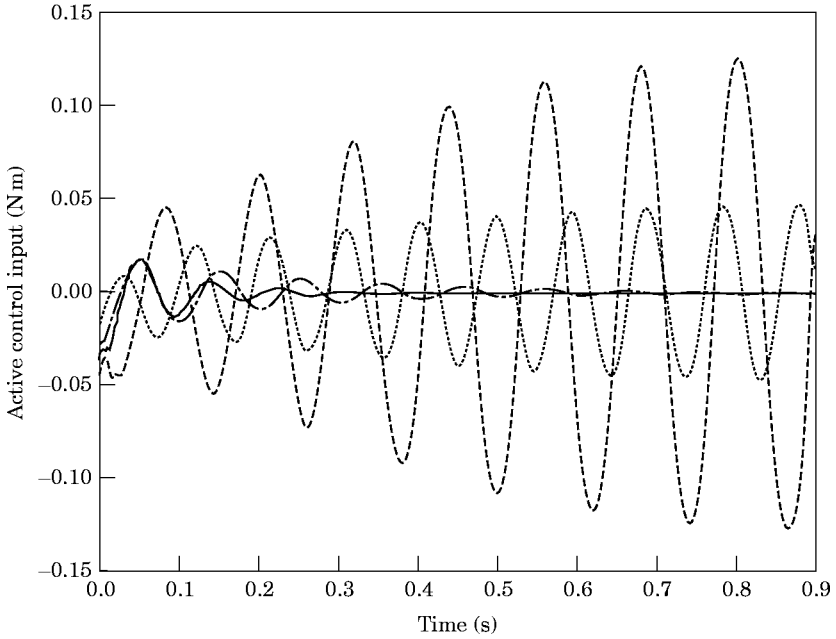

Figure 7. The active control input for various actuator locations with a flow speed of 22 m/s and a weighting parameter of $Q^*/W = 6$. ---, $x/L = 0{\cdot}7$; ···, $x/L = 0{\cdot}2$; –·–, $x/L = 0{\cdot}4$; ——, $x/L = 0{\cdot}5$.

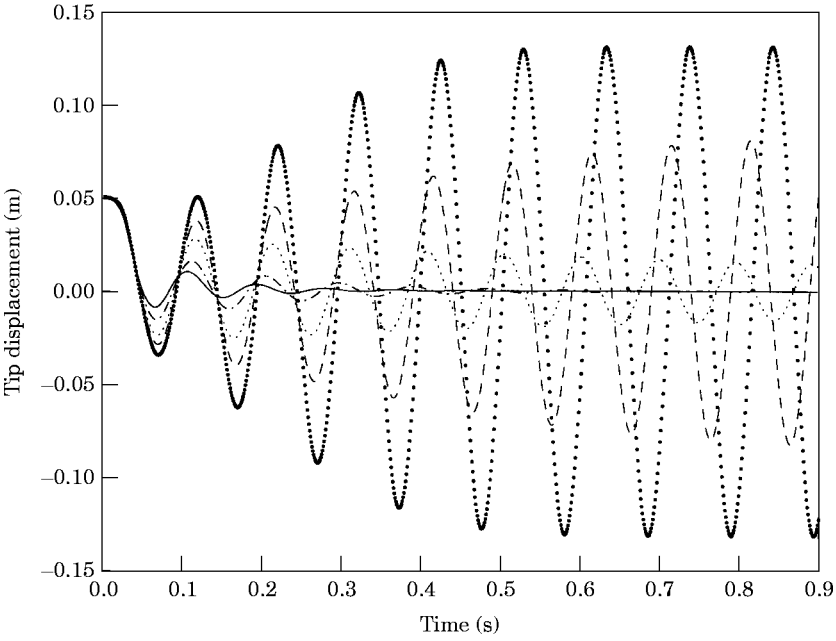

Figure 8. The vertical tip responses for various weighting parameters with a flow speed of 22 m/s and an actuator location of $x/L = 0{\cdot}5$. ●●●, Uncontrolled; – – –, $Q^*/W = 1$; ···, $Q^*/w = 2$; –·–, $Q^*/W = 4$; ——, $Q^*/W = 5$.

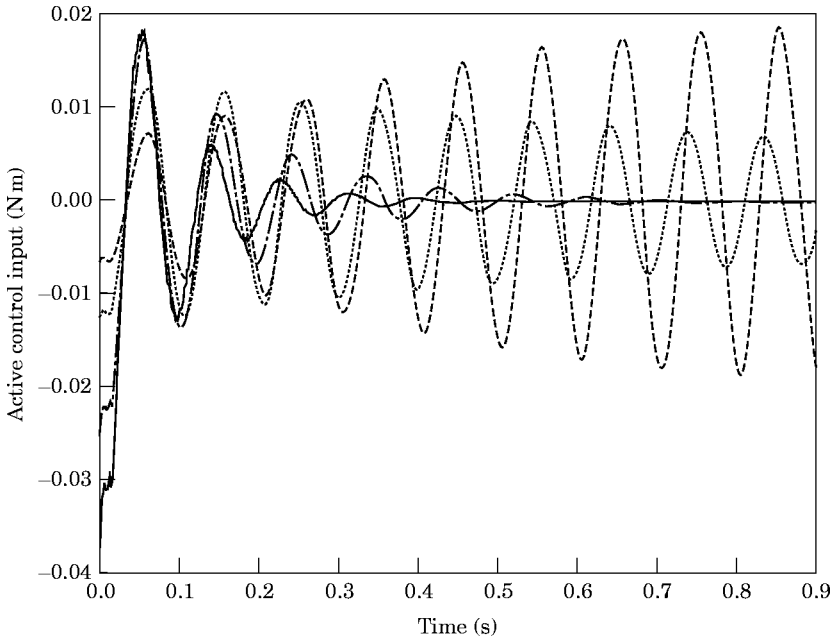

Figure 9. The active control input for various weighting parameters with a flow speed of 22 m/s and an actuator location of $x/L = 0{\cdot}5$. ---, $Q^*/W = 1$; ···, $Q^*/W = 2$; –·–, $Q^*/W = 4$; ——, $Q^*/W = 5$.

matrix. For one control input, W is reduced to represent a scalar quantity. As can be seen in Figure 2, the actuator positioned at the beam center performs better than those located at the other positions. The variation of control cost due to the change of actuator location is more severe in Figure 2 than that in Figure 3. This may be attributed to the nature of

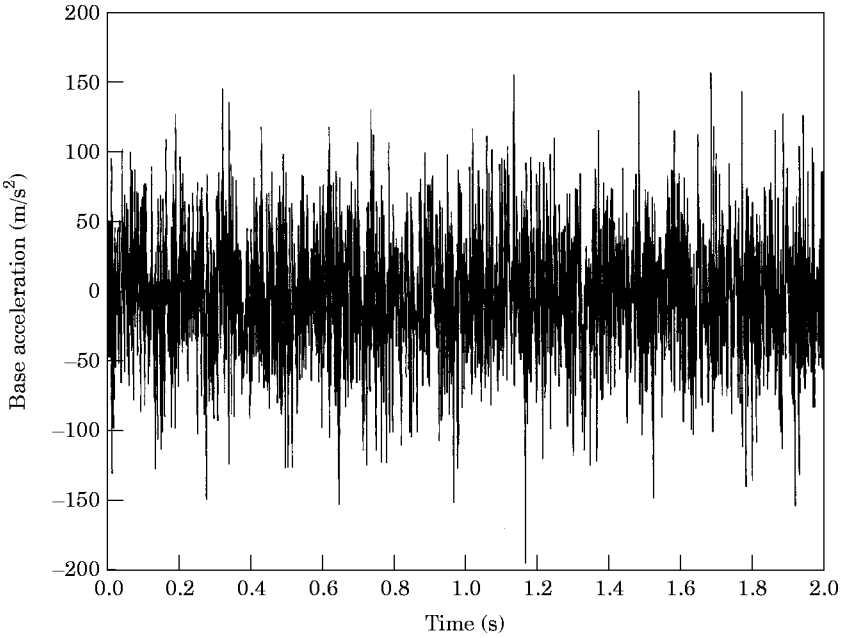

Figure 10. The time history of the random base excitation with a normal distribution.

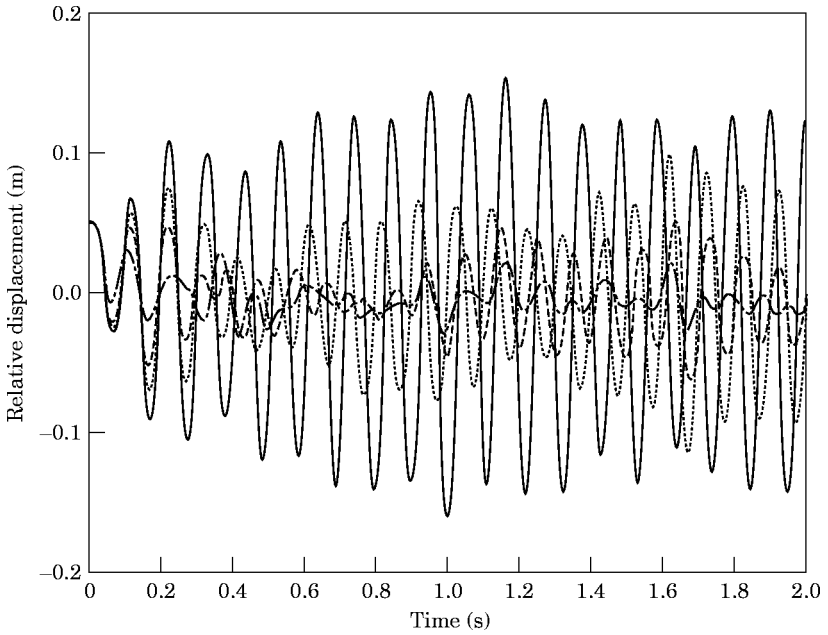

Figure 11. The vertical tip responses of the cantilever pipe subjected to random base excitation for various weighting parameters with a flow speed of 22 m/s and an actuator location of $x/L = 0{\cdot}5$. ——, Uncontrolled; ···, $Q^*/W = 1$; ---, $Q^*/W = 2$; –·–, $Q^*/W = 6$.

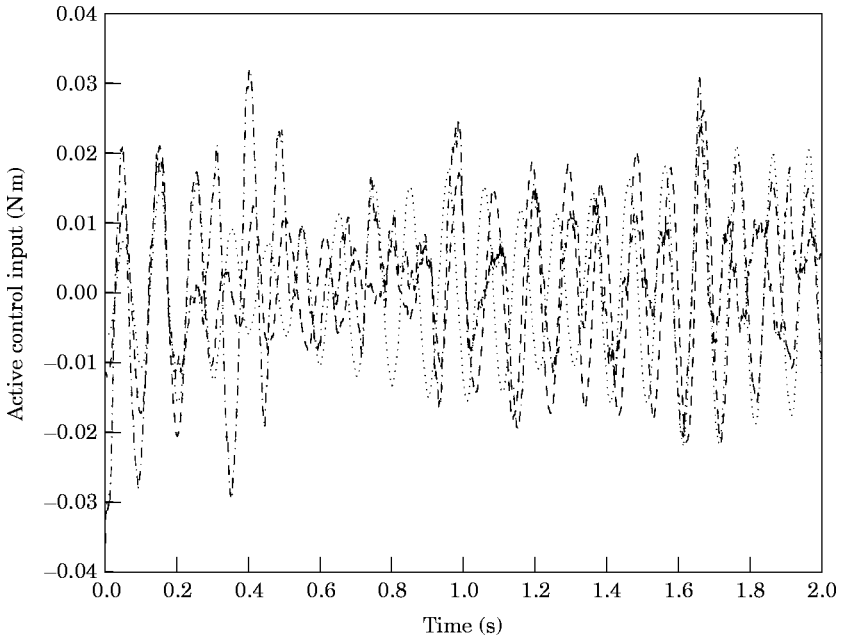

Figure 12. The active control input for the cantilever pipe subjected to random base excitation for various weighting parameters with a flow speed of 22 m/s and an actuator location of $x/L = 0{\cdot}5$. ···, $Q^*/W = 1$; – – –, $Q^*/W = 2$; –·–, $Q^*/W = 6$.

non-proportional damping inherent in the system, which flutters in the second complex mode. For undamped or proportionally damped cantilever pipes, the second mode has one vibration node, which is fixed in space, and the system vibration behaves as a standing wave. However, for fluid conveying cantilever pipes, the gyroscopic damping due to fluid flow is non-proportional and the system vibrates as a travelling wave; that is, the zero crossing, or vibration node, changes with time. Such a change is more severe as the flow speed increases [2]. In Figures 4 and 5 are shown one cycle of vibration for the transverse and rotational displacements, respectively, of the pipe with flow speed 22 m/s. A wide range of change of zero crossing is apparent. Note that for moment type control input, the control is not efficient when the input is near a rotational vibration node.

The vertical tip responses of the fluid conveying cantilever pipe with $Q^*/W = 6$ and a flow speed of 22 m/s for different actuator locations are illustrated in Figure 6. Consistent with that shown in Figure 2, the actuator located at the mid-point of the pipe performs better than those located at other places. The system response without control is included for reference, which shows the pipe vibration, when subjected to disturbance, grows and reaches a steady state amplitude, known as the limit cycle for non-linear system analysis. The corresponding active control input is shown in Figure 7. It is apparent that the actuator position is of vital importance for efficient control. In Figure 8 are shown the effects of the weighting parameter on the vertical tip response of the pipe with a flow speed of 22 m/s and an actuator location of $x/L = 0{\cdot}5$. The corresponding control input is shown in Figure 9. For higher weighting parameter Q^*/W, which means the system response is relatively more important than the control input, more control input is exerted on the system to further suppress vibration of the system. As denoted by a solid line in Figure 8, the pipe vibration is virtually eliminated after 0·3 s. The corresponding peak control input is less than 0·04 N m. Note that for a smaller weighting parameter, such as $Q^*/W = 1$, a smaller control input is used in the instantaneous optimal control process initially.

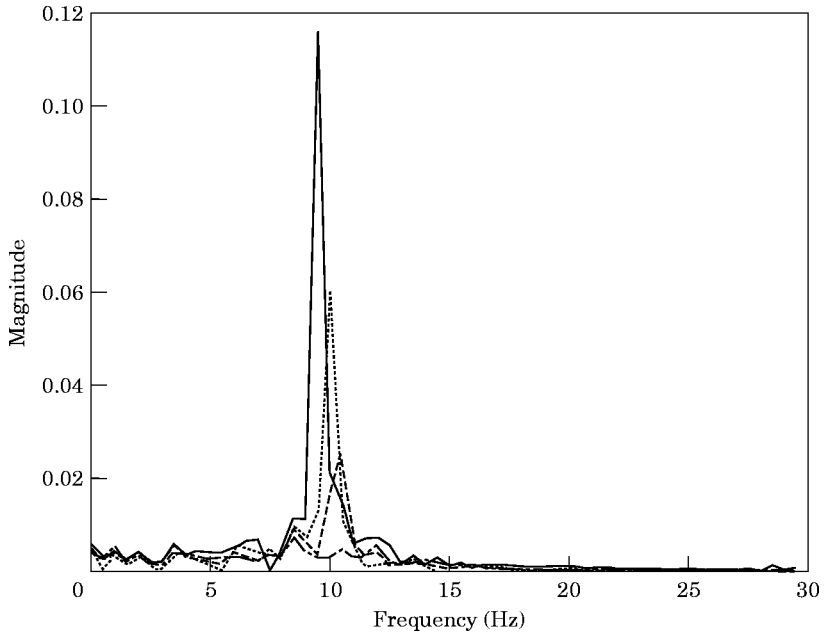

Figure 13. The spectra of the vertical tip responses of the cantilever pipe subjected to random base excitation for various weighting parameters with a flow speed of 22 m/s and an actuator location of $x/L = 0{\cdot}5$. ——, Uncontrolled; ···, $Q^*/W = 1$; ---, $Q^*/W = 2$; –·–, $Q^*/W = 6$.

However, since the vibration of the system is not suppressed sufficiently, a larger control input is needed afterwards due to larger feedback quantities.

The applicability of the control scheme for the fluid conveying cantilever pipe subjected to a random base excitation is assessed. Time history of a random base excitation with normal distribution is shown in Figure 10. In Figure 11 are shown the relative tip displacements with respect to the base motion for various weighting parameters. The flow speed is 22 m/s and the actuator location is $x/L = 0{\cdot}5$. The corresponding control input is shown in Figure 12. The spectra of both the uncontrolled and controlled responses are shown in Figure 13. The peak at around 10 Hz corresponds to the second mode of the fluid conveying pipe, which dominates vibration of the system as the flow speed exceeds the critical value. As can be seen, the control scheme is also capable of mitigating excessive vibration of the pipe when it is subjected to a random base excitation.

5. CONCLUSIONS

The instantaneous optimal closed loop control for vibrational suppression of fluid conveying cantilever pipes has been presented in this work. A large amplitude of vibration, which involves geometric non-linearity, is considered. The non-linear dynamic behaviour of the system is described using the linear equations with fictitious loads applied to account for the kinematic corrections. The non-linear response of the system can then be obtained by using successive co-ordinate transformations. The linear equations of motion are solved using the Newmark method. This formulation avoids the need to construct the tangent damping and stiffness matrices for approximating the non-linear effect. Hence a simpler formulation can be obtained. The importance and determination of the appropriate actuator location has been described. It has been shown that a proper choice of weighting parameter is also important for effective vibration suppression of the pipe system.

The effect of pressurization is not considered in this work. For systems subject to a divergence type of instability, fluid pressure can result in a ''soft'' tube effect; that is, rigidity of the system is reduced. The dynamic behaviour with increasing fluid pressure is the same as that with increasing a compressive force acting at the ends of the pipe. The dynamic response of the system predicted by the theory will then be smaller than that of the real one. As the flow speed varies, the weighting parameters need to be changed accordingly for proper control action. This implies that an adaptive procedure needs to be formulated to adjust the weighting parameters based on the new plant dynamics. This concern warrants further exploration. Experimental work is scarce for the study of vibration control of pipes conveying fluid, especially when the non-linear effects are considered. Future research is called for to undertake such an endeavour for verification of the analytical procedure developed. The effect of actuator location has been examined in this work. However, it is worthwhile to devote separate efforts to develop a procedure for the optimal location of the actuator, especially when multiple control inputs are desired.

ACKNOWLEDGMENT

The authors are grateful to the National Science Council (NSC), Taiwan, ROC, for financial support under contract NSC 85-2212-E-019-002.

REFERENCES

1. G. W. Housner 1952 *Journal of Applied Mechanics* **19**, 205–208. Bending vibrations of a pipe line containing flowing fluid.
2. M. P. Païdoussis and G. X. Li 1993 *Journal of Fluids and Structures* **7**, 137–204. Pipes conveying fluid: a model dynamical problem.

3. T. M. Mulcahy and M. W. Wambsganss 1976 *Shock and Vibration Digest* **8**, 318–332. Flow-induced vibration of nuclear reactor components.
4. R. D. Blevins 1977 *Flow-induced Vibrations*. New York: Van Nostrand Reinhold.
5. A. Shulemovich 1986 *Journal of Applied Mechanics* **53**, 181–186. Flow-induced vibrations caused by roughness in pipes conveying fluid.
6. M. P. Païdoussis, T. P. Luu and B. E. Laithier 1986 *Journal of Sound and Vibration* **106**, 311–331. Dynamics of finite-length tubular beams conveying fluid.
7. C.-L. Chu and Y.-H. Lin 1995 *Shock and Vibration* **2**, 247–255. Finite element analysis of fluid-conveying Timoshenko pipes.
8. P. J. Holmes 1978 *Journal of Applied Mechanics* **45**, 619–622. Pipes supported at both ends cannot flutter.
9. J. Rousselet and G. Herrmann 1981 *Transactions of the American Society of Mechanical Engineers*, *Journal of Applied Mechanics* **48**, 943–947. Dynamic behavior of continuous cantilevered pipes conveying fluid near critical velocities.
10. W. S. Edelstein, S. S. Chen and J. A. Jendrzejczyk 1986 *Journal of Sound and Vibration* **107**, 121–129. A finite element computation of the flow-induced oscillations in a cantilevered tube.
11. J. Tani and Y. Sudani 1992 *The first European Conference on Smart Structures and Materials*, 333–336. Active flutter suppression of a tube conveying fluid.
12. J. Tani and Y. Sudani 1995 *Japan Society of Mechanical Engineers International Journal*, *Series C* **38**(1), 55–58. Active flutter suppression of a vertical pipe conveying fluid.
13. M. Kangaspuoskari, J. Laukkanen and A. Pramila 1993 *Journal of Fluids and Structures* **7**, 707–715. The effect of feedback control on critical velocity of cantilevered pipes aspirating fluid.
14. H. Cui, J. Qui, J. Tani and H. Yanase 1995 *ASME Flow-induced Vibration*, *presented at Pressure Vessels and Piping Conference and Exhibition*, **PVP-298**, 161–166. Robust flutter control of a vertical pipe conveying fluid using gyroscopic mechanism.
15. Y.-H. Lin and C.-L. Chu 1996 *Journal of Sound and Vibration* **196**, 97–105. Active flutter control of a cantilever tube conveying fluid using piezoelectric actuators.
16. J. N. Yang, F. X. Long and D. Wong 1988 *Transactions of the American Society of Mechanical Engineers*, *Journal of Applied Mechanics* **55**, 931–938. Optimal control of nonlinear structures.
17. P. C. Kohnke 1978 *International Journal for Numerical Methods in Engineering* **12**, 1279–1294. Large deflection analysis of frame structures by fictitious forces.
18. N. M. Newmark 1959 *American Society of Civil Engineers*, *Journal of the Engineering Mechanics Division* **85**, 67–94. A method of computation for structural dynamics.
19. D. E. Kirk 1970 *Optimal Control Theory*. Englewood Cliffs, Prentice-Hall.
20. R. D. Cook 1976 *Concepts and Applications of Finite Element Analysis*. New York: John Wiley; second edition.
21. D. B. McIver 1973 *Journal of Engineering Mathematics* **73**, 249–261. Hamilton's principle for systems of changing mass.

APPENIDIX

To formulate the element matrices of the pipe, the displacement fields within an element are interpolated as

$$w = \lfloor N \rfloor \{d_l\}_e, \qquad u = \lfloor U \rfloor \{d_l\}_e, \tag{A1}$$

where w and u are the transverse and longitudinal displacements, respectively, and

$$\lfloor N \rfloor = \lfloor 0 \quad N_1 \quad N_2 \quad 0 \quad N_3 \quad N_4 \rfloor, \qquad \lfloor U \rfloor = \lfloor U_1 \quad 0 \quad 0 \quad U_2 \quad 0 \quad 0 \rfloor,$$
$$\{d_l\}_e = \{u_{l1} \quad w_{l1} \quad \theta_{l1} \quad u_{l2} \quad w_{l2} \quad \theta_{l2}\}^{\mathrm{T}}, \tag{A2}$$

in which

$$N_1 = 1 - 3(x/l)^2 + 2(x/l)^3, \qquad N_2 = x(x/l - 1)^2,$$
$$N_3 = 3(x/l)^2 - 2(x/l)^3, \qquad N_4 = x[(x/l)^2 - x/l],$$

and

$$U_1 = (l - x)/l, \qquad U_2 = x/l, \tag{A3}$$

where $\lfloor N \rfloor$ and $\lfloor U \rfloor$ denote 1×6 row vectors representing shape functions for the transverse displacement and longitudinal displacement, respectively, $\{d_l\}_e$ is the element

nodal degrees of freedom vector, l is the element length, and x is the co-ordinate along the longitudinal direction of the element. The element mass $\mathbf{m}_{p_e}$ and stiffness $\mathbf{k}_{p_e}$ matrices of the pipe can be obtained by using the standard finite element procedure [20]:

$$\mathbf{m}_{p_e} = \mathbf{m}_{t_e} + \mathbf{m}_{a_e}, \qquad \mathbf{k}_{p_e} = \mathbf{k}_{b_e} + \mathbf{k}_{a_e}, \tag{A4}$$

where $\mathbf{m}_{t_e}$ and $\mathbf{m}_{a_e}$ represent the mass matrices for transverse and axial inertia effects; $\mathbf{k}_{b_e}$ and $\mathbf{k}_{a_e}$ denote the stiffness matrices due to bending strain and axial strain respectively. These matrices are combined to form the element mass and stiffness matrices, which can be written as

$$\mathbf{m}_{t_e} = \int_0^l \lfloor N \rfloor^{\mathrm{T}} \mu_p \lfloor N \rfloor \, \mathrm{d}x, \qquad \mathbf{m}_{a_e} = \int_0^l \lfloor U \rfloor^{\mathrm{T}} \mu_p \lfloor U \rfloor \, \mathrm{d}x,$$

$$\mathbf{k}_{b_e} = \int_0^l EI \lfloor N \rfloor_{xx}^{\mathrm{T}} \lfloor N \rfloor_{xx} \, \mathrm{d}x, \qquad \mathbf{k}_{a_e} = \int_0^l EA \lfloor U \rfloor_{x}^{\mathrm{T}} \lfloor U \rfloor_{x} \, \mathrm{d}x, \tag{A5}$$

where μ_p is the mass per unit length of the pipe, E is Young's modulus, I is the area moment of inertia, A is the cross-section area, and the subscript x denotes differentiation. The element mass, damping and stiffness matrices for fluid moving at a constant speed v can be expressed as follows [7]:

$$\mathbf{m}_{f_e} = \mu_f \int_0^l \lfloor N \rfloor^{\mathrm{T}} \lfloor N \rfloor \, \mathrm{d}x + \mu_f \int_0^l \lfloor U \rfloor^{\mathrm{T}} \lfloor U \rfloor \, \mathrm{d}x,$$

$$\mathbf{c}_{f_e} = 2\mu_f v \int_0^l \lfloor N \rfloor^{\mathrm{T}} \lfloor N \rfloor_x \, \mathrm{d}x - \mu_f v \lfloor N \rfloor^{\mathrm{T}} \lfloor N \rfloor \Big|_{x=0}^{x=1},$$

$$\mathbf{k}_{f_e} = \mu_f v^2 \int_0^l \lfloor N \rfloor^{\mathrm{T}} \lfloor N \rfloor_{xx} \, \mathrm{d}x - \mu_f v^2 \lfloor N \rfloor^{\mathrm{T}} \lfloor N \rfloor_x \Big|_{x=0}^{x=l}, \tag{A6}$$

where μ_f is the mass per unit length of the fluid. The last terms on the right sides of the damping and stiffness matrix expressions represent the inflow, at $x = 0$, and outflow, at $x = l$, as the fluid enters the pipe element from one end and exits from the other to account for the fluid boundary conditions [21]. Note that at the free end of the pipe, the outflow terms as depicted above must be added to the structural matrices for correct formulation. The above finite element matrices for both the pipe and the moving fluid can be combined to form the local element matrices. For a pipe exhibiting large deformations, the element fictitious forces $\mathbf{f}_{l_j}$, which are included as part of the element forcing vector $\mathbf{r}_{l_j}$, to account for the kinematic corrections, can be shown to be [17]

$$\mathbf{f}_{l_j} = \begin{Bmatrix} -AE(1-\cos\theta) \\ \dfrac{12EI}{l^2}(\theta - \sin\theta) \\ \dfrac{6EI}{l}(\theta - \sin\theta) \\ AE(1-\cos\theta) \\ \dfrac{-12EI}{l^2}(\theta - \sin\theta) \\ \dfrac{6EI}{l}(\theta - \sin\theta) \end{Bmatrix}. \tag{A7}$$